

ENGINEERING MODELING PROJECT

AARHUS UNIVERSITY
DEPARTMENT OF MECHANICAL ENGINEERING

Hybrid Rocket Project

Shock Diamond Analysis

201271036

Alex Nørgaard

201271088

Afrim Berisha

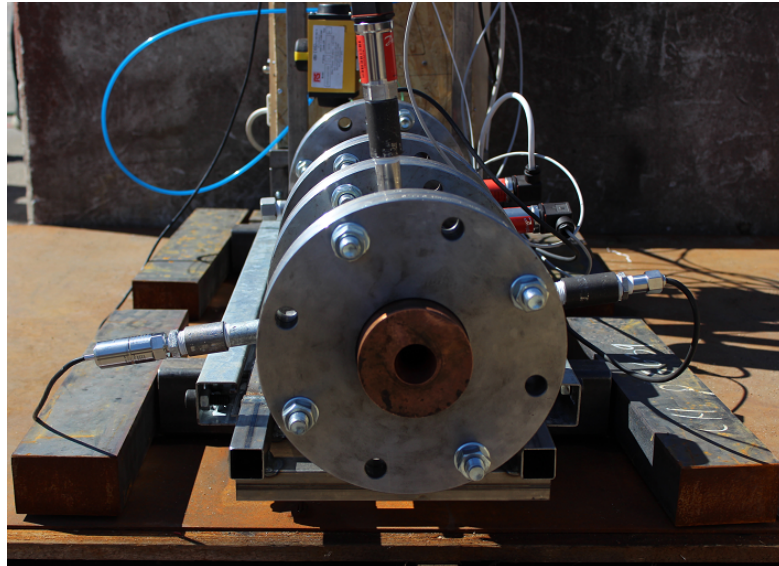
201501385

Guilherme D'Orey

Supervisor:

Gorm Bruun Andresen

3rd June 2016



Contents

1	Introduction	1
2	Basic Hybrid Rocket Theory	2
3	General Nozzle Theory	4
4	General Shock Diamond Theory	9
5	Experiment description	14
6	Results	17
7	Video analysis	19
8	Discussion	22
9	Conclusion	25

1 | Introduction

This project is conducted in the connection of Engineering Modeling Project at Aarhus University. The course is taken as part of the M.Sc in Mechanical Engineering degree. The project concerns a hybrid rocket engine, which has been developed and used in preceding projects.

Two groups of 3 and 4 members have been working together with Peter Madsen, also known as Raketmadsen ("Rocketmadsen") in his Space Laboratory in Copenhagen. The group members of this project were equipped with slow-motion cameras to capture the shock diamonds occurring in the jet whereas the other group focused on analyzing the pressure inside the rocket chamber which will also be used in this project to couple the shock diamonds to the pressure.

1.1 Purpose

It is valuable to have knowledge about how the shock diamonds depend on the chamber pressure so that by analyzing the jet alone, the inside pressure can be calculated. Since the long term goal is to use hybrid rocket engine for manned launch, it is crucial to reduce weight by avoiding measuring devices. The purpose of this project is thus to set up an experiment and analyze the jet from video footage and describe the distance between the shock diamonds as a function of the chamber pressure. This can then be used to calculate the pressure from video footage and thus no use of pressure sensors.

2 | Basic Hybrid Rocket Theory

Rocket engines and jet engines differ from car engines in their way of generating forward motion. Car engines do this by combustion of fuel and converting up/down motion to rotational motion, which is transferred to the wheels by a series of mechanical links. In contrast, rocket- and jet engines generate propulsion by ejecting a medium at high speeds and essentially using Newton's 3rd law of motion, which is known as:

$$F = m \cdot \frac{dv}{dt} \quad (2.1)$$

With time dependent mass and constant exit velocity this can be rearranged to give:

$$F = \frac{d(m)}{dt} \cdot v = \dot{m} \cdot v \quad (2.2)$$

Where \dot{m} is mass flow rate out of the engine and v is the speed of the ejected matter. Rocket engines develop this ejected gas by mixing fuel with an oxidizer in a combustion chamber resulting in expansion towards the nozzle and thus supersonic exit speeds and thereby thrust. They differ from jet engines in their way of accessing the matter. Jet engines (or more generally *duct propulsion* engines) use the surrounding medium as "working fluid" in combination with some fuel, while rocket engines store the matter. This gives rise to different kinds of rocket propulsion concepts:

- Liquid rocket engines keep the oxidizer and fuel as liquid in two separate tanks.
- Solid rocket engines use solid oxidizer and fuel.
- Hybrid rocket engines use solid fuel and liquid oxidizer.

Hybrid rocket engine is to be used in the present project.

The idea of the hybrid rocket is to inject the liquid oxidizer, in this case H_2O_2 , under high pressure into the precombustion chamber, which consists of potassium

permanganate ($KMnO_4$) resulting in the following chemical reaction:



The contact between the oxidizer and $KMnO_4$ results in a highly exothermic chemical reaction, which raises the temperature to around 600 K and above the autoignition temperature of the fuel grain. This rise in temperature yields in rising pressure as well. The high pressure is utilized in the nozzle throat, which is a converging-diverging nozzle (de Laval nozzle). The gas is pushed through the converging part under high pressure and can only expand again after exiting the nozzle through the diverging part. This expansion of gas accelerates it to supersonic speed and – by Newton's 3rd law – generates thrust. Due to the pressure loss, there has to be high pressure in the oxidizer tank in order to maintain continuous injection and thus continuous thrust. An overview of a hybrid rocket engine can be seen on figure 2.1¹.

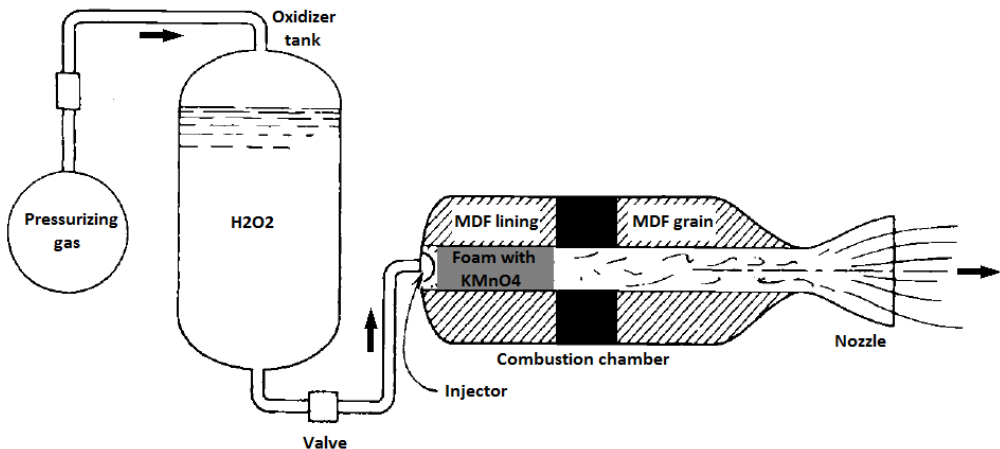


Figure 2.1: Overview of a hybrid rocket engine

[source ?](#)

¹ Rocket Propulsion Elements, George P. Sutton and Oscar Biblarz, 7th edition, p. 10.

3 | General Nozzle Theory

The nozzle is one of the main components that categorize a rocket propulsion system.

In this chapter the main characteristics of the Nozzle and the theory behind is going to be explained.

3.1 Converging-diverging nozzle

The converging-diverging nozzle, or de Laval nozzle, named after the inventor Gustaf de Laval, is a tube, where the cross section area in the beginning decreases (the converging part) and then increases (the diverging part) (see figure 3.1¹). The section that separates this two parts is called the throat. This kind of nozzle is widely used to accelerate the flow and can have different sizes with varying ratio between the sections depending on the application.

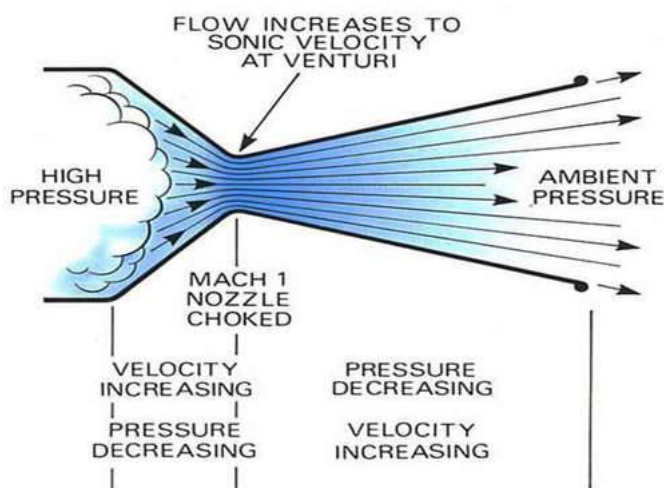


Figure 3.1: De Laval nozzle

¹<http://nandang-smart.blogspot.dk/2009/06/gas-turbine-engine-theory.html>

3.2 Ideal rocket simplifications

By assuming an ideal rocket a more simple analysis can be done, which are close to the real rocket performance, with the real rocket 1 to 6% below of the ideal rocket performance. The assumptions are²:

1. The working substance (or chemical reaction products) is homogeneous.
2. All the species of the working fluid are gaseous. Any condensed phases (liquid or solid) add a negligible amount to the total mass.
3. The working substance obeys the perfect gas law.
4. There is no heat transfer across the rocket walls; therefore, the flow is adiabatic.
5. There is no appreciable friction and all boundary layer effects are neglected.
6. There are no shock waves or discontinuities in the nozzle flow.
7. The propellant flow is steady and constant. The expansion of the working fluid is uniform and steady, without vibration. Transient effects (i.e., start up and shut down) are of very short duration and may be neglected.
8. All exhaust gases leaving the rocket have an axially directed velocity.
9. The gas velocity, pressure, temperature and density are all uniform across any section normal to the nozzle axis.
10. Chemical equilibrium is established within the rocket chamber and the gas composition does not change in the nozzle (frozen flow).
11. Stored propellants are at room temperature. Cryogenic propellants are at their boiling points.

Thermodynamic relations

These are the main equations that build up the the equations applied to the nozzle, which are:

The mass conservation equation:

$$\frac{d\dot{m}}{dt} = 0 \quad \Leftrightarrow \quad \frac{d\rho v A}{dt} = 0 \quad (3.1)$$

²Rocket Propulsion Elements, George P. Sutton and Oscar Biblarz, 7th edition, p. 46.

Where: \dot{m} = Mass flow, ρ = Density, v = Velocity and A = Cross sectional area.

The enthalpy in an adiabatic flow:

$$h_2 - h_1 = 0.5(v_2^2 - v_1^2) = c_P(T_2 - T_1) \quad (3.2)$$

Where: H = Specific enthalpy, c_P = Specific heat capacity (for constant pressure) and T = Temperature.

The ideal gas law:

$$pV = RT \quad (3.3)$$

Where: p = Pressure, V = Volume and R = Gas constant.

The ratio between the specific heat:

$$k = \frac{c_P}{c_V} \quad (3.4)$$

Where: c_V = Specific heat capacity (for constant volume).

The Mach number:

$$M = \frac{v}{c} = \frac{v}{\sqrt{kRT}} \quad (3.5)$$

Where: c = The speed of sound.

3.2.1 Isentropic flow

In the ideal rocket there is no friction in the flow and it can thus be considered isentropic. Under this assumption it is possible to define equations that relate the stagnation temperature (T_0) and stagnation pressure (p_0).

Temperature:

$$\frac{T_0}{T} = [1 + 0.5(k - 1)M^2] \quad (3.6)$$

Pressure:

$$\frac{P_0}{P} = [1 + 0.5(k - 1)M^2]^{\frac{k}{(k-1)}} \quad (3.7)$$

Density:

$$\frac{\rho_0}{\rho} = p [1 + 0.5(k - 1)M^2]^{\frac{k}{(k-1)}} \quad (3.8)$$

These are important relations, because it is possible to know the local properties, if the Mach number is known. The stagnation properties are the ones in the combustion chamber, where the velocity is zero. Then, the area ratio is a ratio between the cross sectional area of the throat and the cross sectional area elsewhere

in the nozzle, taking account eq.(3.1), (3.5) and (3.8), the area ratio in terms of Mach numbers is:

$$\frac{A_2}{A_1} = \frac{M_1}{M_2} \sqrt{\left[\frac{1 + 0.5(1 - k)M_2^2}{1 + 0.5(1 - k)M_1^2} \right]^{\frac{k+1}{k-1}}} \quad (3.9)$$

This correlation gives a very important factor in the nozzle, as it is possible to see on figure 3.2. In subsonic flow, the area ratio diminishes (that is the converging part) and rises to Mach 1 upon reaching the throat section.

So two important factors are taken from this. The flow velocity rises until Mach 1 in the converging part, and only reaches supersonic velocities in the diverging part if and only if Mach 1 is reached in the throat. Otherwise it will work like a Venturi tube.

As mentioned before, the temperature, pressure and density change along the nozzle as shown in figure 3.3³.

Using equation (3.1), (3.2) and (3.6) it is possible to write the exit velocity, which can be used to calculate the thrust:

$$v_e = \sqrt{\frac{2k}{k-1} RT_1 \left[1 - \left(\frac{p_e}{p_1} \right)^{\frac{k-1}{k}} \right] + v_1^2} \quad (3.10)$$

On figure 3.3 and by eq. (3.2) and eq. (3.10) it is possible to see that the temperature lowers, when the velocity rises. That means the heat energy is being converted to kinetic energy.

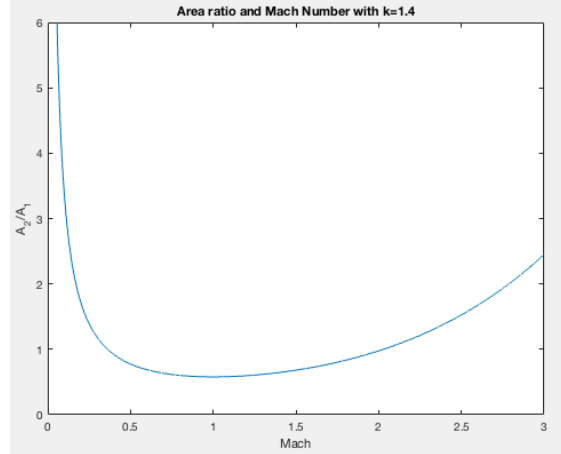


Figure 3.2: Mach number and area ratio.

³Rocket Propulsion Elements, George P. Sutton and Oscar Biblarz, 7th edition, p. 56.

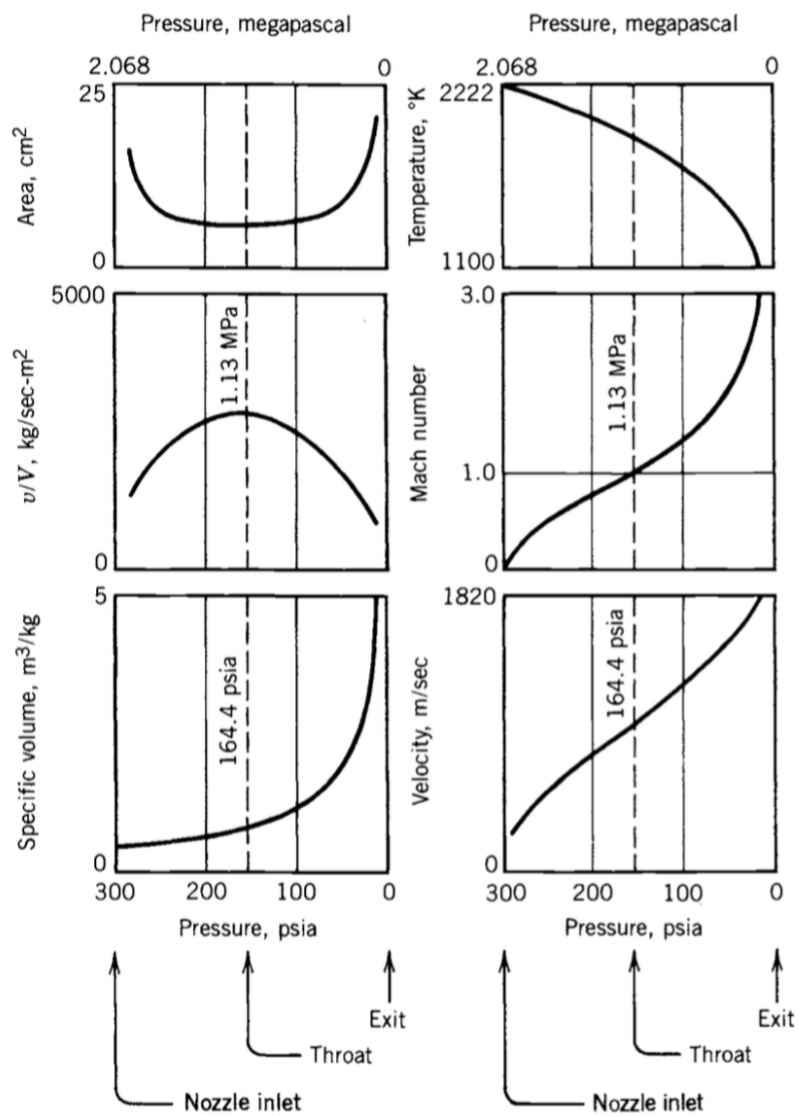


Figure 3.3: Variation of pressure with temperature, Mach number and specific volume.

4 | General Shock Diamond Theory

In all types of jet engines and rocket engines, where flow is leaving the nozzle with supersonic speed, a phenomenon referred to as "shock diamonds" occurs in the jet. Here a special structure of shock waves and pressure lines are made due to a pressure difference between the jet and the atmosphere. This results in one of two situations as shown below (see table 4.1)¹.

Table 4.1: Pressure link

1.	$P_e < P_a$	Overexpanded
2.	$P_e > P_a$	Underexpanded

Where P_e = Exhaust pressure and P_a = Atmospheric pressure.

4.1 Overexpanded

When the atmospheric pressure is higher than the exhaust pressure, the flow leaving the nozzle will be forced to turn towards the center axis of the plume (see figure 4.1¹). When doing this it passes an oblique (or angled) shock wave, which compresses the flow and increases the pressure. Also a normal shock wave, a so-called Mach disk, is formed in the jet increasing the pressure of the flow even higher. Passing through the Mach disk increases the temperature as well, which causes unburned fuel to ignite making the diamond visible. Eventually, at some point the pressure is high enough to exceed the atmospheric pressure forcing the flow to turn back outwards. This is made possible because of a process called Prandtl-Meyer expansion waves (or fans), which occurs when the supersonic flow is travelling around the convex corner/edge of the oblique shock wave. When the expansion waves reach the center axis, they are meeting their "twins", causing

¹<http://www.aerospaceweb.org/question/propulsion/q0224.shtml>

them to shoot back towards the boundary of the jet. Then hitting the boundary of the jet reflects the expansion waves in such a way, that they switch into Prandtl-Meyer compression waves, which subsequently merges to an oblique shock wave. When the flow travels through the different Prandtl-Meyer waves, it first redirects to become parallel to the center axis and is afterwards turning inwards again helping the oblique shock wave to produce another Mach disk. This procedure repeats itself as long as the merging of the compression waves is strong enough to produce another shock wave. Also, a turbulent layer caused by friction between the jet and the free air eventually will end the jet and thus the formation of shock diamonds.

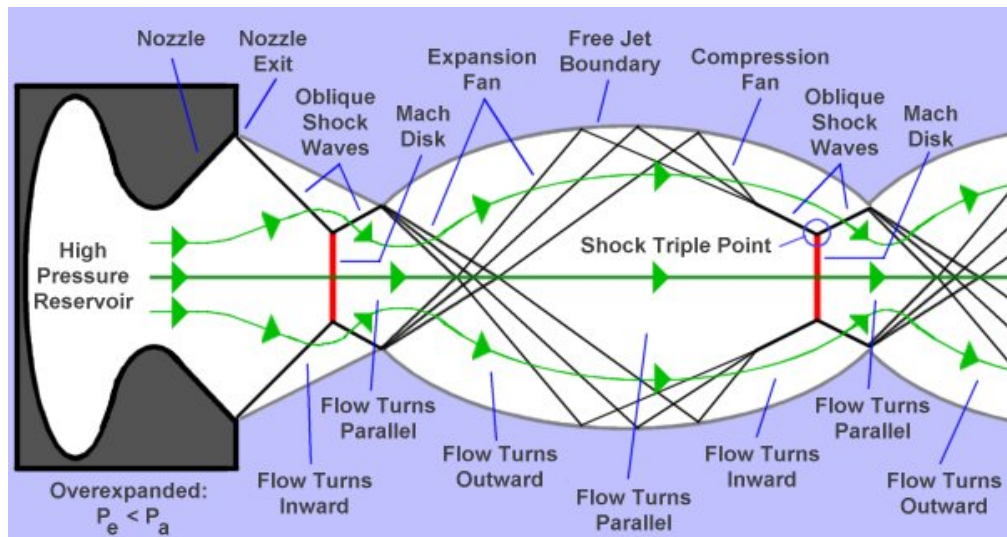


Figure 4.1: Overexpanded jet.

4.2 Underexpanded

When the atmospheric pressure is lower than the exhaust pressure, the flow will unlike prior turn outwards (see figure 4.2²). When the flow travels around the edge of the nozzle, it creates expansion waves that behave as before, resulting in an oblique shock wave. The rest of the process and appearance of the jet are executed as mentioned above, but due to the difference in the two cases, the distance to the first shock diamond is also different.

²<http://www.aerospaceweb.org/question/propulsion/q0224.shtml>

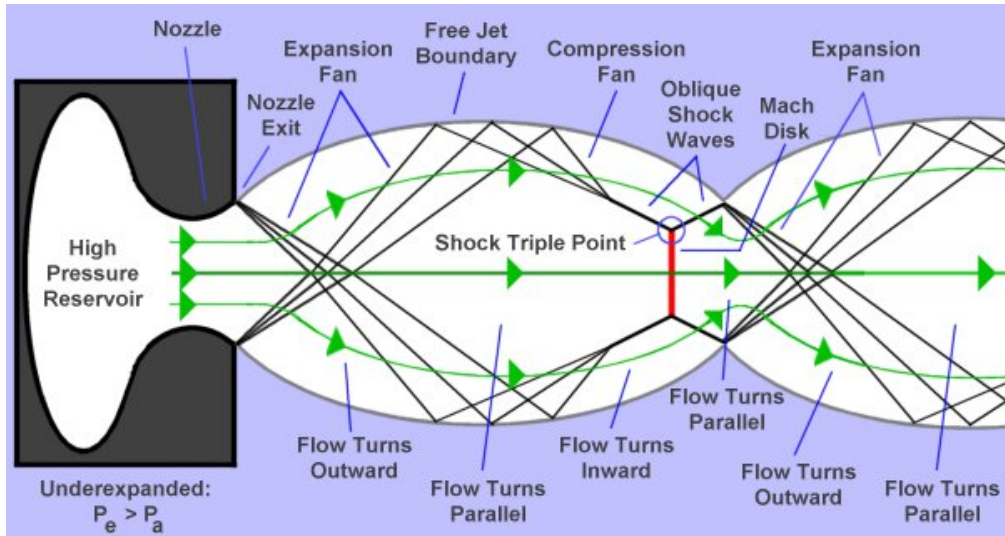


Figure 4.2: Underexpanded exhaust plume

4.3 Distance from pressure measurements

As part of investigating shock diamonds in the jet, there exists an equation from jet theory³ to calculate an approximated distance to the first diamond (see eq. (4.1)):

$$\frac{x}{d_e} \approx 0.67 \left(\frac{p_0}{p_a} \right)^{0.5} \quad (4.1)$$

Where D_0 = Nozzle diameter, P_0 = Exhaust/stagnation pressure which can be set to the pressure measured in the afterburner by assuming the velocity inside the chamber to be zero. Finally P_a = Atmospheric pressure.

This equation is empiric and thus made from a number of experiments. A variation in the test setup could therefore lead to imbalance between the equation and the actual distance, which makes it essential to investigate the derivation of it further. To do so the Mach number in the nozzle exit Ma_e is calculated with eq. (4.2):

³Exhaust of Underexpanded Jets from Finite Reservoirs, M.M. Orescanin, D. Prisco and J.M. Austin, July 2010, p. 10.

$$\frac{A_t}{A_e} = Ma_e \left[\frac{\frac{(k+1)}{2}}{1 + \left[\frac{(k-1)}{2} \right] Ma_e^2} \right]^{\frac{(k+1)}{2(k-1)}}$$

$$\frac{356.3 \text{ mm}^2}{890.9 \text{ mm}^2} = Ma_e \left[\frac{\frac{(1.4+1)}{2}}{1 + \left[\frac{(1.4-1)}{2} \right] Ma_e^2} \right]^{\frac{(1.4+1)}{2(1.4-1)}}$$

$$\Rightarrow Ma_e = 2.44$$
(4.2)

Where A_t = Cross sectional area of the throat, A_e = Cross sectional area of the nozzle exit and k = Ratio of specific heat capacity, which is assumed to be 1.4. From literature⁴ a number of experimental results leads to several curves, which is reprinted and shown in figure 4.3.

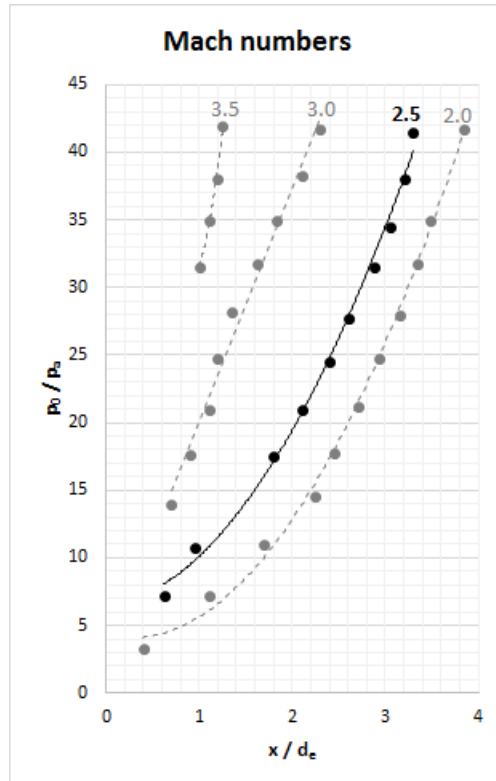


Figure 4.3: Mach numbers

The figure is made from experiments done on a nozzle with a divergence angle of 10° , whereas this report deals with an angle of 15° . However, it is also known

⁴ *Journal of the aeronautical sciences*, Donald E. Wilcox, Alexander Weir, Jr., J.A.Nicholls and Roger Dunlap, February 1957, p. 152.

that the divergence angle has little influence on the Mach number over most of the pressure range⁵. Therefore it is decided that the black line in figure 4.3 representing a Mach number of 2.5 is reasonably close for comparison with the calculated number of 2.44. With this decision made figure 4.4 is drawn, where the axis of figure 4.3 are switched and only the linear part of the curves kept. Also, eq. (4.1) is added to the plot (red).

Written in the form of eq. (4.1), a Mach number of 2.5 thus gives the new approximated equation below (see eq. (4.3)), which is used in chapter 6.

$$\frac{x}{d_e} \approx 0.21 \left(\frac{p_0}{p_a} \right)^{0.75} \quad (4.3)$$

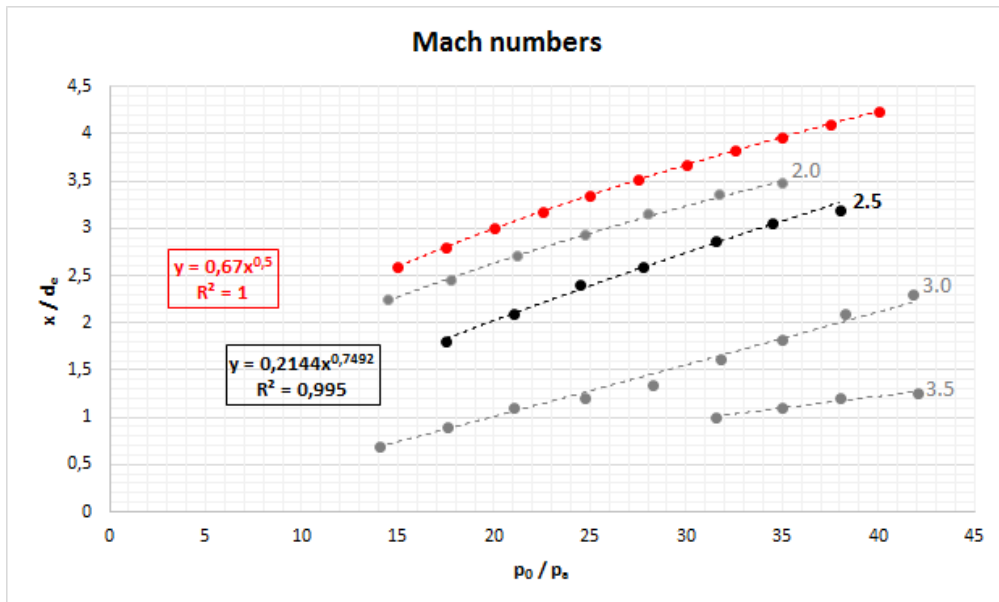


Figure 4.4: Mach numbers - Linear parts

⁵Journal of the aeronautical sciences, Donald E. Wilcox, Alexander Weir, Jr., J.A.Nicholls and Roger Dunlap, February 1957, p. 152.

5 | Experiment description

The experiments took place in Peter Madsen's Space Lab, in Copenhagen, from the 3rd to the 4th of May, 2016.

The rocket was fixated in a metal frame horizontally, in front of a concrete block to prevent the rocket from moving under test. As a matter of safety a wooden box was placed on top of the rocket and then covered by sand bags, in a way that would not affect the experimental results.

5.1 Pressure sensors

The rocket was mounted with eight pressure sensors, from which three were located on the afterburner chamber. One on each side and one on top with different reading frequencies of $250Hz$, $2000Hz$ and $10000Hz$. Another three of the sensors were mounted in the preburning chamber, two with a reading frequency of $250Hz$ and one with $10000Hz$. The remaining two sensors were placed in the tank of hydrogen peroxide. One of $250Hz$ and one of $10000Hz$. The sensor's signal was then connected with LabVIEW to a mirror computer controlled by another computer placed in a safe zone, where the measurements were recorded.

5.2 Camera recording

To record the jet for later analysis of the distances between the shock diamonds, a Go Pro Hero black® camera was placed 2.35 meters away from the nozzle center. The camera was set to record in 240 FPS and 720p during the tests, and a ruler was placed behind, where the jet would pass, to serve as a reference with black and white stripes of 5cm each.

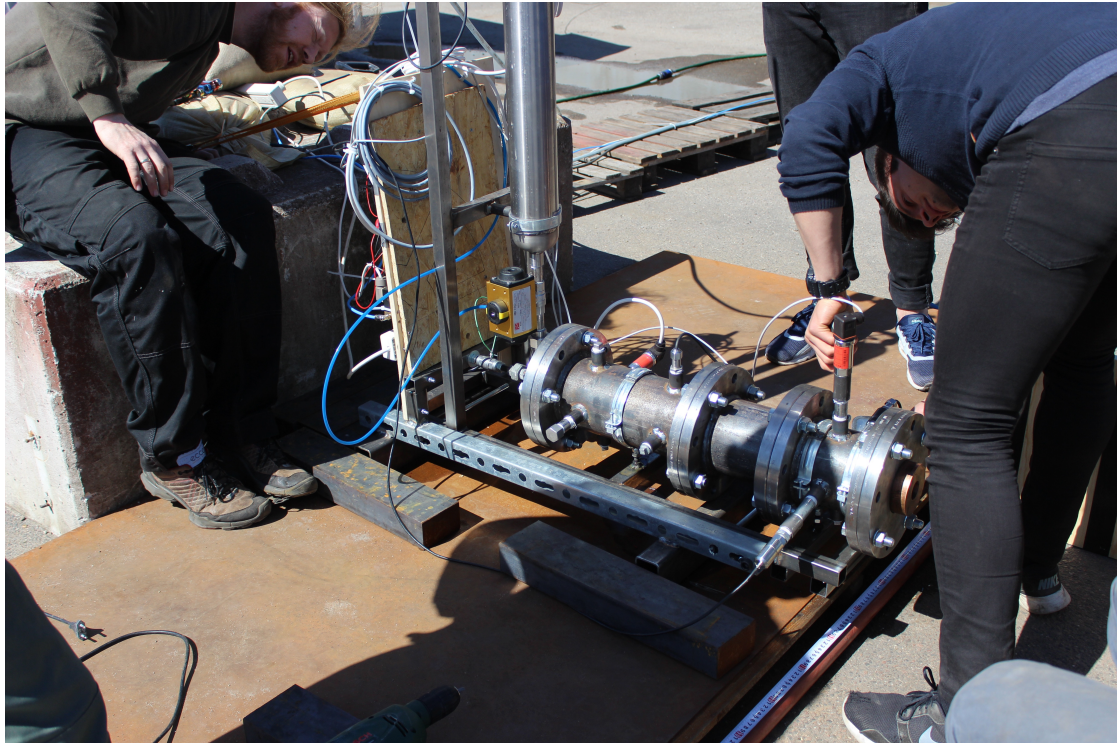


Figure 5.1: The rocket with the pressure sensors connected.

5.3 Preparation for the test

For each test a procedure had to be followed to guarantee success of the test and safety of participants.

First some foam was treated with potassium permanganate and then inserted in an MDF block, which was then placed in the preburning chamber. Then the chamber was sealed with a pneumatic nut runner. Another MDF block was inserted in the combustion chamber, which was then sealed as well.

The next step was to fill the tank with the oxidizer, and since hydrogen peroxide is highly flammable only the necessary persons were nearby the rocket, with everyone else placed in the safety zones. When the tank was full, it was pressurized and the remaining persons were sent to the safety zone to wait for the countdown.



Figure 5.2: The rocket covered with sandbags with the ruler and the camera.

6 | Results

The outcome of the two test days was a total of 4 successful tests with pressure measurements at 8 different locations on the engine. The relevant results of this is presented below. In addition, the jet was recorded in slow-motion with the analysis of this covered in chapter 7.

6.1 Pressure curves

The different pressure measurements was done with 3 types of sensors with each of their own measuring frequency: *Low* – 250Hz , *Middle* – 2000Hz and *High* – 10000Hz . For later comparison the middle one is chosen, because the video recording is only 240FPS. The reason for not choosing the low one is a desire for bigger precision, especially at pressure spikes, however the high recording frequency would be excessive rate of measurement. With the sensor type chosen, the measured data for the 4 burns are plotted in MATLAB as shown in fig. 6.1 with the raw data in the upper one. Due to a big amount of noise the lower shows the same data, but with an average of every 2000 values to make a smoother plot, though with lower pressure spikes at the beginning.

6.2 Distance curves

By using eq. (4.1) from chapter 4 it is possible to convert the pressure to the distance for the first shock diamond. The resulting distances of the raw pressure data are thus shown in the top plot of fig. 6.2, and as before an average of every 2000 values is plotted in the bottom one.

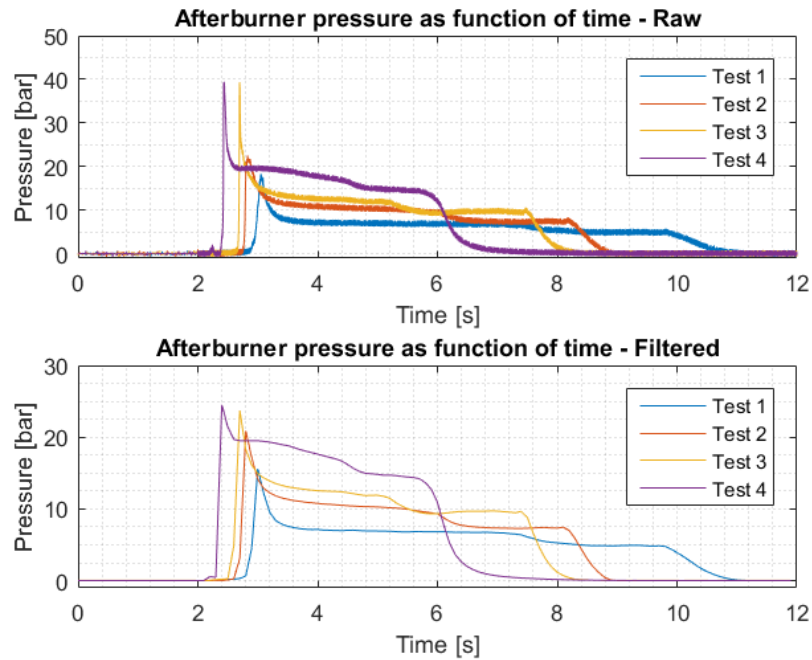


Figure 6.1: Pressure plots

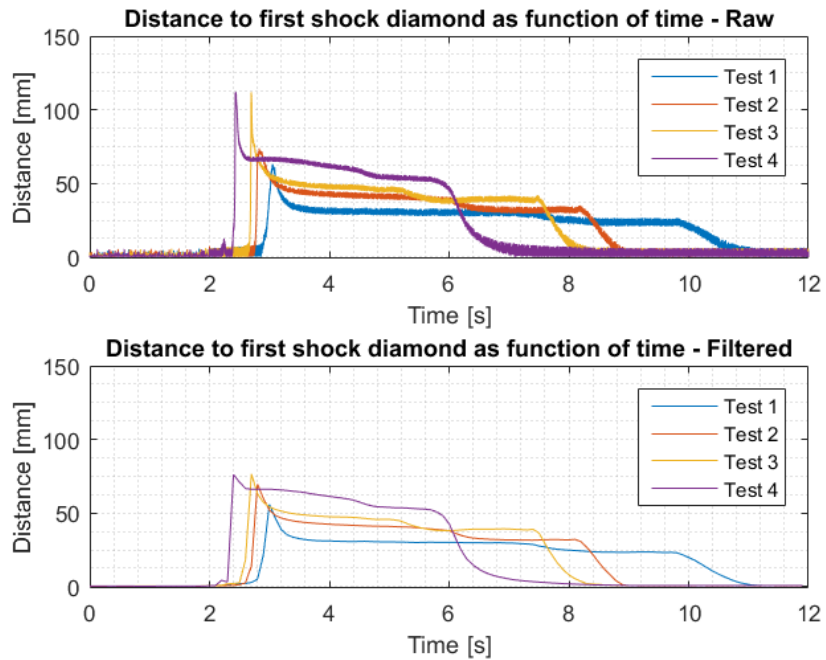


Figure 6.2: Distance plots

7 | Video analysis

In order to calculate the distances to the shock diamonds, a cropped version of the slow motion footage is imported to MATLAB. Here it is decomposed to frames, which are then used to monitor the images frame by frame. Furthermore, it is possible to decompose the colours into RGB (Red, Green, Blue) colours. The colour intensities are plotted along a line going through the jet. This is shown on figure 7.1.

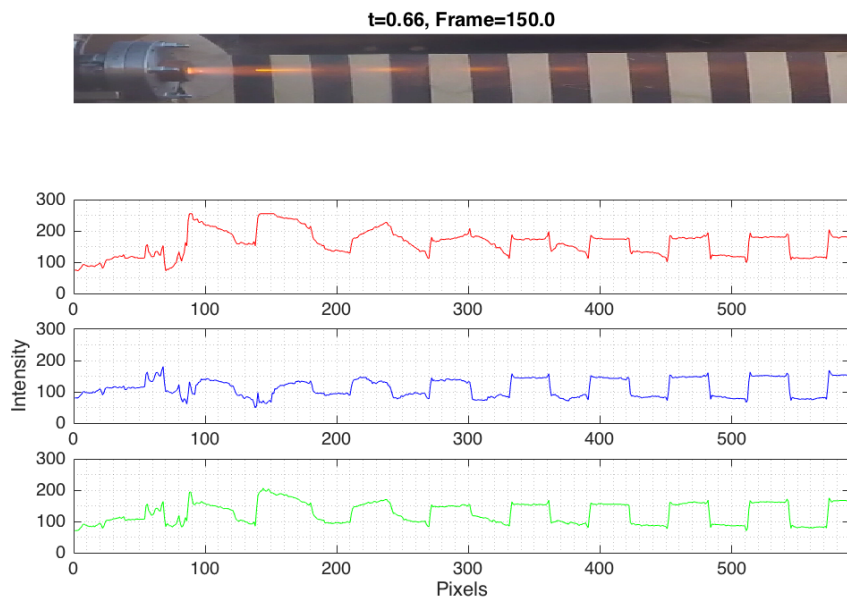


Figure 7.1: Slow motion footage decomposed to frames and RGB colours.

By utilizing the fact that the shock diamonds are more visible than the rest of the jet, it is possible to locate them by searching for pixels with higher intensity.

Since the jet is mainly orange coloured it is logical to search for rise in the red colour intensity. This can be used to manipulate the relevant pixels and thus mark the shock diamonds, as seen on figure 7.2. Here the red and blue colours are intensified to give the shock diamonds a magenta colour.



Figure 7.2: Marking of shock diamonds by raising red and blue intensity.

Since the ruler in the background is made of black and white it will affect the colour intensities, which explains the periodic peaks on figure 7.1. This noise is manually removed in MATLAB so the diamonds are isolated. The diamond positions can thus be plotted as peaks, which can be seen on figure 7.3. It is important to clarify, that the height of the peak is not relevant and thus does not reflect the intensity of the colour. It is used to locate the shock diamond positions exclusively.

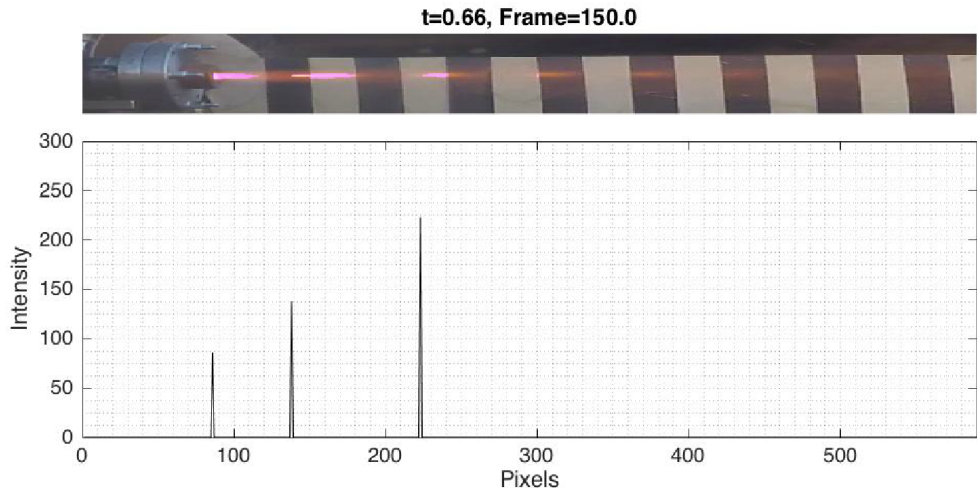


Figure 7.3: Peaks locating the position of nozzle exit, the first and the second shock diamond.

To convert the distance from pixels to millimeters the nozzle is used as reference frame. Since the nozzle diameter is actually 90mm but 60 pixels in the video footage, the following relation can be derived:

$$ratio = \frac{real \ diameter}{video \ diameter} = \frac{90mm}{60pixels} = 1.5 \frac{mm}{pixel} \quad (7.1)$$

Thus one pixel in the video equals 1.5mm in reality. Furthermore the duration of 1 frame can be calculated to be $\frac{1}{240}s$ since the recording speed is 240 FPS. From this knowledge, the distance between the diamonds can be plotted in millimeters as a function of time, which is shown on figure 7.4.

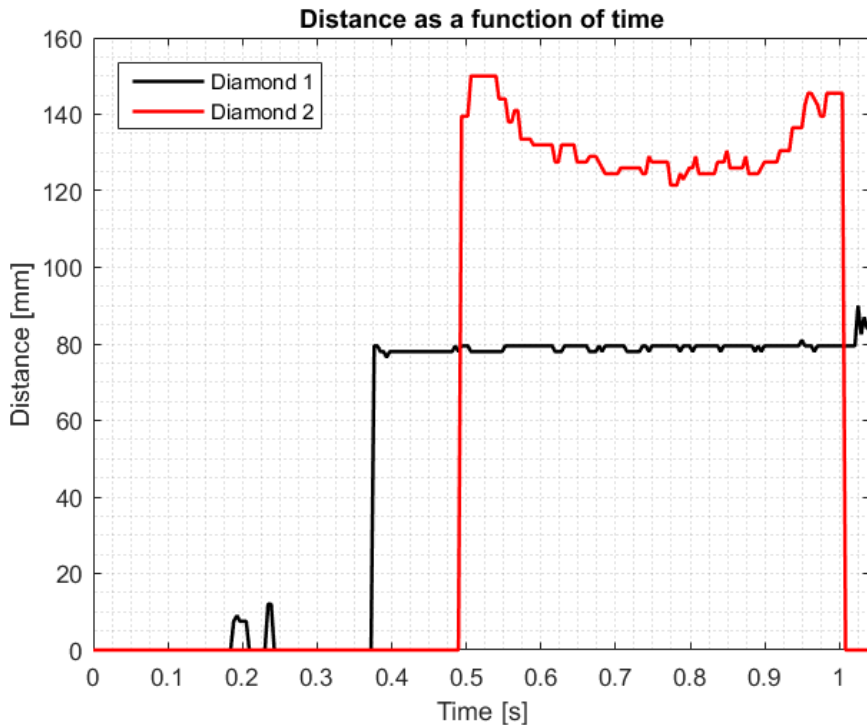


Figure 7.4: Distance as a function of time.

The figure shows the distance between the nozzle and the first diamond depicted as a black line and the distance between the first and second diamond as a red line. The mean distance to the first diamond is 79.2mm and the mean distance between the first and second diamond is 132.3mm.

Furthermore the figure shows two peaks occurring around 0.2 seconds. By inspecting the video and the data analysis simultaneously it shows, that this is due to a combination of nozzle displacement and reflection of the jet onto a bolt and is not treated further.

8 | Discussion

With results from both the pressure and the video analysis, it is now possible to compare the two. Combination of the distance plots from previous sections can be seen on figure 8.1.

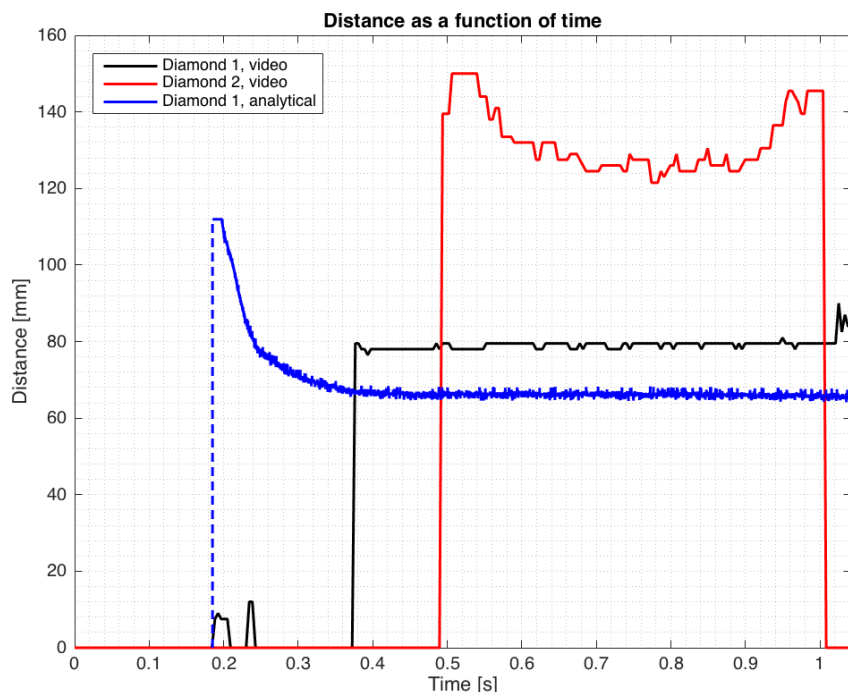


Figure 8.1: Plot of distances from pressure results and video analysis.

Due to the fact that there were unequal number of data points between the black and blue line it was necessary to take the mean value of the analytical- and video analysis distances respectively before calculating the error. This gives the result in eq. (8.1).

$$Error = \frac{|x_{analytical} - x_{video}|}{x_{analytical}} \cdot 100 = 20.0\% \quad (8.1)$$

Since the curves are almost constant with little fluctuation within the area of interest the manner of calculating the error with mean values is assumed to be reasonably exact.

The reason for this error percentage can be linked to different sources or errors:

- Background ruler

The ruler which was meant for distance measuring resulted in noise due to the colour difference between the black and white stripes. Furthermore this influenced the colour intensity of the shock diamonds and thus the potential to localize them.

- Camera distance

Since the diamonds appeared within a distance of 1 meter from the nozzle the camera could have been placed closer to the rocket engine and thus focus on the area where the shock diamonds occur. Yet the reason for placing at the chosen distance was due to heat exposure to the camera, which turned out to be an unnecessary safety precaution. The reason for not moving the camera closer in later experiments was to keep the footage consistent.

- Camera angle

The camera was not placed at the exact same height as the jet, which changed the appearance of the shock diamonds. Furthermore the lateral angle to the shock diamonds contributed to this effect.

- Camera resolution

Since the video had to be recorded in highest possible framerate of 240 FPS, the resolution was 720p. This made the shock diamonds and the nozzle blurry. Given that the nozzle was used as reference for distance measurements this could give rise to errors.

- Analytical equation

The analytical equation used for comparison was taken for a Mach number of 2.5, whereas the calculated Mach number for the rocket engine was 2.44. This could give rise to wrong coefficients used in the equation.

With the sources of errors known it is interesting to study how the ideal equation would look like. Since eq. (4.1) is a power function it is possible to estimate a similar equation for the results from the experiments. This is done by doing power

regression on the measured chamber pressure and the distance to the first shock diamond found from the video analysis.

This results in eq. (8.2):

$$\frac{x}{d_e} = 1.22 \left(\frac{p_0}{p_a} \right)^{0.22} \quad (8.2)$$

Plot of this equation together with the results from the video analysis can be seen on figure 8.2.

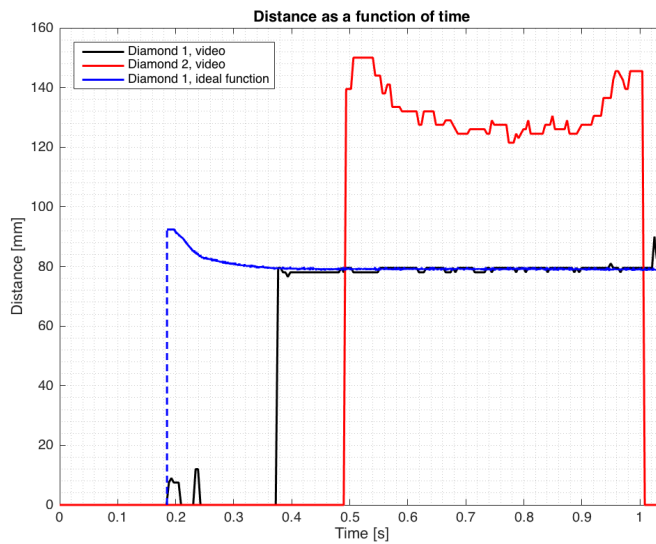


Figure 8.2: Ideal equation for distance to shock diamond 1.

Rewriting eq. (8.2) to eq. (8.3) it is now possible to calculate the chamber pressure from the measured distances making a pressure sensor unnecessary.

$$\frac{p_0}{p_a} = \left(\frac{x}{1.22 d_e} \right)^{\frac{1}{0.22}} \quad (8.3)$$

Deriving a similar equation for the distance to shock diamond 2 based on present results is not possible due to the unsuitable shape of the curve. The reason for this shape could be that the appearance (and thus size) of the shock diamond changes with each frame starting faint, building up and fading out again towards the end. An equation for shock diamond 2 would have made it possible to find a relation between the first and second shock diamond. This could have been possible if the ruler was replaced by a uniform background.

9 | Conclusion

The project's purpose was to set up and experiment and analyze the distances between the shock diamonds.

The experiments were conducted over 2 days and resulted in 4 burns from which number 4 had the best video footage and thus had the best foundation for analyzing the shock diamonds. By using the pressure measurements and an analytical equation for the distance to the first shock diamond, it was possible to plot pressure and distance curves as a function of time.

Subsequently a video analysis was made on the collected footage using MATLAB. This resulted in distance plots, which showed a distance of 79.2mm from nozzle to the first diamond and 132.3mm from the first to the second diamond. This is a 20% deviation from the analytical calculations for the first shock diamond. For the present results it is not possible to couple the distance to the pressure for the second shock diamond and therefore an error cannot be calculated.

The reason for this error is believed to be experiment setup and equipment accuracy, mainly because of the ruler in the background.

Based on the present results an ideal equation was estimated from the measured pressure and the distances from the video analysis. This gives the ability to calculate the chamber pressure from the distance on the video.